Published in final edited form as:
Proteins. 2011 February ; 79(2): 581–597. doi:10.1002/prot.22907.

Distinct Second Extracellular Loop Structures of the Brain Cannabinoid CB_1 Receptor: Implication in Ligand Binding and Receptor Function

Joong-Youn Shim[1,*], **James Rudd**[1], and **Tomas T. Ding**[2]

[1]J. L. Chambers Biomedical/Biotechnology Research Institute, North Carolina Central University, Durham, North Carolina 27707

[2]Department of Pharmaceutical Sciences, Biomanufacturing Research Institute and Technology Enterprise, North Carolina Central University, Durham, North Carolina 27707

Abstract

The G-protein coupled receptor (GPCR) second extracellular loop (E2) is known to play an important role in receptor structure and function. The brain cannabinoid (CB_1) receptor is unique in that it lacks the inter-loop E2 disulfide linkage to the transmembrane (TM) helical bundle, a characteristic of many GPCRs. Recent mutation studies of the CB_1 receptor, however, suggest the presence of an alternative intra-loop disulfide bond between two E2 Cys residues. Considering the oxidation state of these Cys residues, we determine the molecular structures of the 17-residue E2 in the dithiol form ($E2_{dithiol}$) and in the disulfide form ($E2_{disulfide}$) of the CB_1 receptor in a fully hydrated 1-palmitoyl-2-oleoyl-*sn*-glycero-3-phosphocholine (POPC) bilayer, employing a combination of simulated annealing (SA) and molecular dynamics (MD) simulation approaches. We characterize the CB_1 receptor models with these two E2 forms, $CB_1(E2_{dithiol})$ and $CB_1(E2_{disulfide})$, by analyzing interaction energy, contact number, core crevice and cross-correlation. The results show that the distinct E2 structures interact differently with the TM helical bundle and uniquely modify the TM helical topology, suggesting that E2 plays a critical role in stabilizing receptor structure, regulating ligand binding, and ultimately modulating receptor activation. Further studies on the role of E2 of the CB_1 receptor are warranted; particularly comparisons of the ligand-bound form with the present ligand-free form.

Keywords

G-protein coupled receptor (GPCR); second extracellular loop (E2); simulated annealing (SA); molecular dynamics (MD); transmembrane (TM); helical topology; toggle switch

INTRODUCTION

Brain cannabinoid (CB_1) receptors are G-protein coupled receptors (GPCRs)1 and belong to the rhodopsin-like subfamily.2 Members of this integral membrane protein (IMP) family are characterized by seven transmembrane (TM) helices (TMH) (H1-H7) connected by three intracellular loops (I1-I3) and three extracellular loops (E1-E3). Located in the highly polar environment of the membrane-water interfacial region of a lipid bilayer,3 the GPCR loops are not restricted by the membrane4 and are known to be important for stabilizing the multi-

[*]To whom correspondence should be addressed at J. L. Chambers, Biomedical/Biotechnology Research Institute, North Carolina Central University, 700 George Street, Durham, NC 27707, USA., Phone: 919-530-7763; Fax: 919-530-7998; jyshim@nccu.edu.

spanning receptor,5–7 most likely in a sequence-specific manner.[8] In particular, E2, as part of the binding pocket, is known to play a central role in integrating ligand binding into receptor activation.[7,9–13]

Even within the rhodopsin family of GPCRs, E2 structures vary. The X-ray structure of rhodopsin[14] shows that E2, containing a β-sheet lid, is deeply inserted into the receptor TM helical core and completely covers the binding pocket thereby restricting solvent access. In contrast, the X-ray structures of the β-adrenergic receptors (βARs)[15,16] and the adenosine A_{2A} receptor ($A_{A2}R$)[17] show that E2, containing a short α-helical segment, is displaced away from the receptor core and partially covers the binding pocket thereby allowing solvent access. Further, it has been shown that E2 can achieve distinct conformations upon agonist and antagonist binding for modulating receptor function.[18,19]

Several studies on the cannabinoid receptors[20,21] demonstrate that E2 is important for ligand binding and receptor function. However, with little structural information available the structural determination of the 17-residue E2 of the CB_1 receptor is quite challenging due to its conformational flexibility,[22] location in the membrane-water interface, and conformational sensitivity to its anchoring positions at the TM helical ends. This challenge is partially ameliorated by several popular secondary prediction programs, including PSIPRED,[23] JPRED3[24] and APSSP2,[25] that correctly predict the presence of the E2 helical segment found in the X-ray structures of βARs[15,16] and suggest the presence of a helical segment within E2 in the CB_1 receptor (Table I).

Of interest, the CB_1 receptor is unique in that it lacks the inter-loop disulfide bond between E2 and H3, common to many GPCRs, which is known to be important for maintaining the correct receptor structure and function[26–28] through the coupling between the extracellular loop and the TM helical core domains.[29] The absence of the inter-loop disulfide bond in the CB_1 receptor, due to the absence of the H3 Cys residue, makes E2 less inserted into the receptor core region and the TM helical bundle more closely packed thereby limiting water access to the crevice.[30] Recent mutation studies of the CB_1 receptor, however, suggest the presence of an alternative intra-loop disulfide linkage between two E2 Cys residues.[21,31]

In the present study, we determine E2 structure of the CB_1 receptor by employing a combination of simulated annealing (SA) and molecular dynamics (MD) simulation approaches. We use the recently developed homology model of the CB_1 receptor TM helical bundle,[32] which provides the precise boundaries of the TMH, to aggressively explore the E2 conformations in detail, and the predicted E2 secondary structure (Table I) as a molecular constraint to reduce the conformational space. Considering the reduced state and the oxidized state of E2 (i.e., E2 with two Cys residues in the dithiol form ($E2_{dithiol}$) and in the disulfide form ($E2_{disulfide}$)) separately, we determine the CB_1 receptor structures with these two E2 conformations, named $CB_1(E2_{dithiol})$ and $CB_1(E2_{disulfide})$, in a fully hydrated 1-palmitoyl-2-oleoyl-*sn*-glycero-3-phosphocholine (POPC) bilayer. The results show that the distinct E2 structures, interacted differently with the receptor bundle, uniquely modify the TM helical topology: $E2_{dithiol}$, with two helical turns, isolated from TMH, which interferes less with the packing of the TM helical bundle, leading to the attachment of H5 to H3; and $E2_{disulfide}$, with one helical turn and a cyclic ring enclosed by the disulfide linkage, closely packed to TMH, which interacts more with the TM helical bundle, leading to the detachment of H5 from H3. The results of the present studies suggest the critical role of E2 in stabilizing the receptor, regulating ligand binding by allowing or preventing access to the crevice, and ultimately modulating receptor function. In the present manuscript, a numbering, similar to the Ballesteros-Weinstein numbering is used[33]; TM helical residues and the loop position for every loop residue are indicated by superscription.

MATERIALS AND METHODS

MD simulations

For the CB_1 receptor system necessary for exploring the E2 conformation, we used the recently developed homology model of the CB_1 receptor in a fully hydrated POPC bilayer,[32] which resulted in a system size of 80 Å × 98 Å × 98 Å. All simulations of the CB_1 receptor in a POPC bilayer were performed by the NAMD simulation package (http://www.ks.uiuc.edu/Research/namd/)[34] using CHARMM22 force field parameters with the CMAP correction for the ϕ/ψ angles[35,36] for the protein and the TIP3 water model,[37,38] and CHARMM32 force field parameters for the lipids.[39] The topology definitions and the parameters for the palmitoylated Cys residue (CYP), including the parameters around the bond connecting C415 of the CB_1 receptor and the carbonyl carbon of the palmitoyl moiety, as used in the literature,[40] were found in the NAMD ParameterTopologyRepository site (http://www.ks.uiuc.edu/Research/namd/wiki/index.cgi?ParameterTopologyRepository). The temperature was maintained at 310 K through the use of Langevin dynamics[41] with a damping coefficient of 1/ps. The pressure was maintained at 1 atm by using the Nosé-Hoover method[42] with the modifications as described in the NAMD User's Guide (http://www.ks.uiuc.edu/Research/namd/2.6/ug/). The van der Waals interactions were switched at 10 Å and zero smoothly at 12 Å. Electrostatic interactions were treated using the PME method.[43] A pair list for calculating the van der Waals and electrostatic interactions was set to 13.5 Å and updated every ten steps. A multiple timestepping integration scheme, the impulse-based Verlet-I (r-RESPA) method,[44] was used to efficiently compute full electrostatics. The timestep size for integration of each step of the simulation was 1 fs.

Conformational searches of the CB_1 receptor E2

Two separate conformational searches of the CB_1 receptor E2 in a POPC bilayer were performed: one of $E2_{dithiol}$; and the other of $E2_{disulfide}$. Employing an SA approach similar to the protocol by Fiser et al.[45], we sampled the conformation of $E2_{dithiol}$ (i.e., $W255^{E2}$-$I271^{E2}$) by constraining the predicted consensus sequence ($C257^{E2}$ – $C264^{E2}$) (Table I) to be an ideal α-helix by applying torsional constraints (ϕ = −57 degrees and ψ = −47 degrees) using adaptive biasing force46 as implemented in NAMD.47 To save CPU time, a rectangular box (40 Å × 40 Å × 35 Å), large enough to accommodate any change associated with the conformational change of the targeted E2, was defined and only atoms inside the box were simulated while the atoms outside the box were held fixed. Further, the backbone atoms of E1 and E3 as well as the TM helical residues other than the side chain atoms within one helical turn from the extracellular boundaries were also held fixed. The simulation was performed in the constant volume (NVT) ensemble.

The SA cycle consisted of the following steps: energy minimization using 1,000 steps; heating to 2,510 K in 15 ps; MD simulation at 2,510 K for 20 ps; cooling down gradually to 310 K within 60 ps; MD simulation at 310 K for 20 ps; and then energy minimization using 2,000 steps. By repeating the SA cycle, a total of 166 energy-minimized E2 conformations were collected, for which a hierarchical (pairwise average linkage) cluster analysis, using MaxCluster (http://www.sbg.bio.ic.ac.uk/~maxcluster/index.html), was performed resulting in 16 clusters with a maximum inter-cluster distance of 0.7. By visual inspection, seven clusters that showed similar positions for the E2 helical segment and a cluster in which the E2 helical segment stayed far off the helical bundle were eliminated. For the remaining eight clusters, representative conformations were selected for further exploration: the number of the conformation in each cluster was 5, 4, 2, 1, 1, 1, 1, and 1, respectively, which in part reflected their relative abundance in the cluster. The number of the structure at each step of the conformational search procedure is summarized in Table II.

The CB_1 receptor model[32] whose E2 was replaced by each of these sixteen E2 conformations was embedded in a POPC bilayer and subjected to a 5 ns to 20 ns MD simulation in the constant pressure (NPT) ensemble without any constraint to relieve any poor geometry on the E2 anchor regions connecting H4 and H5 and to examine the stability of the E2 helical segment. Any of the resulting E2 conformations for which the helical segment became unstructured or stayed far off the helical bundle was dropped from further examination. The E2 C-terminal residues of the remaining four distinct conformations were then remodeled by ModLoop (http://modbase.compbio.ucsf.edu/modloop/modloop.html).[45] The resulting structures were subjected to an additional MD simulation and the validity of the modeled E2 structures was examined by WHAT IF (http://swift.cmbi.kun.nl/whatif/).[48]

The conformational search protocol for $E2_{disulfide}$ was almost the same as for $E2_{dithiol}$. For this conformational search, two E2 Cys residues were connected to form a disulfide bond. By the fold recognition program GenTHREADER (http://bioinf.cs.ucl.ac.uk/psipred/),[49] a suitable fold containing the disulfide-enclosed cyclic segment (i.e., $C257^{E2}$-$C264^{E2}$) and the α-helical segment ($C257^{E2}$ – $C260^{E2}$) was identified from the X-ray structure of the human NOTCH2 (PDB code: 2OO4).[50] During the SA simulation, this fold was constrained by using adaptive biasing force46 as implemented in NAMD.47 A total of 115 energy-minimized E2 conformations were collected from the SA simulations during which the disulfide-enclosed cyclic segment was constrained. These 115 conformations were then grouped into twenty eight clusters. Seventeen clusters were then eliminated due to the disulfide-enclosed cyclic segment either straying too far off of the helical bundle or occupying too similar a position. For the remaining eleven clusters, representative conformations were selected for further exploration: the number of the conformation in each cluster was 2, 1, 1, 1, 1, 1, 1, 1, 1, 1, and 1, respectively (Table II). The CB_1 receptor model[32] whose E2 was replaced by each of these twelve E2 conformations was embedded in a POPC bilayer and further refined by MD simulation as described for $E2_{dithiol}$.

Data analysis

The MD analysis software g_correlation (http://www.mpibpc.mpg.de/home/grubmueller/downloads/GeneralizedCorrelations/index.html)[51] was used to create cross-correlation matrices from ~ 12,000 coordinates recorded every 2 ps from the last 24 ns MD simulations of $CB_1(E2_{dithiol})$ and $CB_1(E2_{disulfide})$, respectively. Both the least square fit and the non-linear generalized correlation were calculated using the Cα atoms of the receptor residues. To minimize any loss of the detail of interest from the full protein, the N-terminal end residues before H1 and the C-terminal end residues after H7 were not considered in this analysis.

Aromatic stacking was defined as any two aromatic residues (i.e., Phe, Tyr, Trp, or His) for which the distance between the two aromatic ring centroids was less than 8 Å. To determine the concentration of stacking within a range along the z-axis, the z-coordinate of one of the residues participating in the interaction was used; the remaining residue's coordinates were not considered.

The binding core crevice diameter was calculated using the HOLE program (http://hole.biop.ox.ac.uk/hole), developed to measure the pore radius of ion channels.[52] Sampling was done every 0.5 Å along the z-axis and a midpoint (i.e., c-point) between H2, H3, and H7 that was dynamically determined for every coordinate was used to define the core crevice at the extracellular region.

Circular dichroism spectroscopy of the CB_1 receptor E2 peptide

$E2_{disulfide}$ and $E2_{dithiol}$ of the peptide WNCEKLQSVCSDIFPHI were custom synthesized (> 95 %) by ProImmune (Oxford, UK) and used without further purification. The peptides were dissolved in phosphate buffered saline (PBS, 10 mM phosphate, pH 7.4) at a concentration of 0.1 mg/ml (50 μM). Far UV circular dichroism (CD) spectra were collected on a JASCO J815 spectrophotometer at ambient temperature using 0.1 cm cuvette. Fifty acquisitions were made for each spectrum. Deconvolution of the recorded spectra was accomplished using the CONTIN L analysis program with reference set 3, provided by Dichroweb (http://dichroweb.cryst.bbk.ac.uk).[53]

RESULTS

Conformational analysis of the CB_1 receptor with two distinct E2

The sampled 166 conformations of $E2_{dithiol}$ and 115 conformations of $E2_{disulfide}$ occupied similar extracellular regions formed by H3/H4/H5, leaving the region near H2/H6/H7 relatively unoccupied (Fig. 1). After clustering analyses and the ensuing MD simulations, the final eight, four from each E2 form, that contained an α-helical segment, as predicted (Table I), were obtained. These E2 conformations were classified into two distinct conformational classes with respect to the spatial orientation of the α-helical segment within E2: in class **A** the α-helical segment is parallel to the membrane surface, as seen in the X-ray structures of βARs,[15,16] while in class **B** it is perpendicular to the membrane. Class **A** represents the majority of the high helicity $E2_{dithiol}$ having two helical turns, while class **B** represents the majority of the low helicity $E2_{disulfide}$ having only one helical turn.

Conformation **A1** of $E2_{dithiol}$ and conformation **B3** of $E2_{disulfide}$ were chosen as the best conformations of each E2 form based upon receptor stability and the degree of molecular interactions with the other regions of the receptor (data shown in Fig. S1 & Table SI). The CB_1 receptor models with these two E2 conformations (i.e., $CB_1(E2_{dithiol})$ and $CB_1(E2_{disulfide})$) were subjected to long MD simulations for further examination. The rest of our studies are discussed based upon the MD simulation results of these two CB_1 receptor models. The root mean-square deviations (RMSDs) show that the TM helical bundle of $CB_1(E2_{dithiol})$ quickly converges in 20 ns of the simulation, while the TM helical bundle of $CB_1(E2_{disulfide})$ is slow to converge even at the end of the simulation (Fig. 2A). It appears that large fluctuations of E2 in $CB_1(E2_{disulfide})$ throughout the simulation cause the rest of the receptor to fluctuate accordingly. The helical backbone RMSDs of $CB_1(E2_{dithiol})$ are 0.5 Å higher than those of $CB_1(E2_{disulfide})$ due to the large outward movement of H1 at the extracellular region from the helical bundle. Differences in structural convergence shown in $CB_1(E2_{dithiol})$ and $CB_1(E2_{disulfide})$ indicate distinct E2 structures play a role in altering the receptor stability.

Structural features of two distinct E2 conformations

A close examination of E2 in $CB_1(E2_{dithiol})$ and $CB_1(E2_{disulfide})$ exhibits a combination of stabilizing interactions, including hydrophobic interactions, salt bridges, H-bonding interactions, and aromatic stacking interactions (Fig. 2B). E2 in $CB_1(E2_{dithiol})$ contains a helical segment (i.e., $C257^{E2}$-$V263^{E2}$), as seen in the X-ray structures of βARs,[15,16] in an amphipathic alignment: the polar face, exposed to water, is stabilized by a salt bridge by $E258^{E2}$/$R186^{3.22}$ and a H-bond by $Q261^{E2}$/$D184^{E1}$, while the non-polar face, buried in the receptor core, is stabilized by forming a hydrophobic cluster with the E2 non-polar residues (i.e., $W255^{E2}$, $C257^{E2}$, $L260^{E2}$, $C264^{E2}$, $F268^{E2}$ and $P269^{E2}$). In $CB_1(E2_{dithiol})$, several salt bridges, including $R182^{E1}$/$D176^{2.63}$/$K192^{3.28}$/$D184^{E1}$, $R186^{3.22}$/$E258^{E2}$ and $D266^{E2}$/$K370^{E3}$, exist at the receptor extracellular region (Fig. 2Bi and Table III). Additionally,

F268^{E2} of E2 in CB$_1$(E2$_{dithiol}$) is involved in a network of aromatic stacking at the receptor extracellular region (see below).

E2 in CB$_1$(E2$_{disulfide}$) contains a short helical segment (i.e., C257^{E2}-L260^{E2}) due to the geometric constraint by the disulfide bond that interferes with α-helix formation. Salt bridges by D266^{E2}/K183^{E1} and E258^{E2}/R186$^{3.22}$ contribute to E2 and receptor stabilization and the cyclic ring enclosed by the disulfide linkage is stabilized by several H-bonds: N256^{E2}/K259^{E2}, N256^{E2}/L260^{E2}, C257^{E2}/Q261^{E2} and E258^{E2}/R186$^{3.22}$ (Fig. 2Bii and Table III). Two intra-loop hydrophobic clusters (i.e., one: W255^{E2}, L260^{E2}, C264^{E2} and L271^{E2} and another: C257^{E2}, I267^{E2}, F268^{E2} and P269^{E2}) on the top of the TM helical bundle appear to minimize the exposure to water and contribute to receptor stabilization. P269^{E2} also forms an inter-loop hydrophobic cluster with the TM residues L190$^{3.26}$, L193$^{3.29}$ and L253$^{4.62}$, suggesting that the C-terminal of E2 in CB$_1$(E2$_{disulfide}$) is closely packed to TMH. Finally, the aromatic network at the receptor extracellular region in CB$_1$(E2$_{disulfide}$), which is formed by the E2 aromatic residues F268^{E2} and H270^{E2}, is highly extensive (see below).

Considering that the square of each buried hydrophobic surface area is estimated to contribute to the free energy of protein folding (24 cal/mol),[54] the E2 hydrophobic residues folded into the receptor core significantly contribute to receptor stabilization. Similarly, considering that multiple salt bridges compensate for the loss of entropy by a single salt bridge,55 the multiple salt bridges centered at D176$^{2.63}$/K192$^{3.28}$ in CB$_1$(E2$_{dithiol}$) and by D184^{E1}/K192$^{3.28}$ and E258^{E2}/R186$^{3.22}$ in CB$_1$(E2$_{disulfide}$) appear to be important for receptor stabilization. In support, recent mutation studies suggest that D176$^{2.63}$ and D184^{E1} of the CB$_1$ receptor contribute to receptor structure and function through charge interaction.[56,57]

CD spectroscopy of the E2 peptide of the CB$_1$ receptor

It is well known that a-helical secondary structure gives rise to a positive CD-band (positive ellipticity) at 195–196 nm and two negative bands around 209 and 222 nm. The CD-spectrum of E2$_{dithiol}$ displayed a positive band at 195 nm and a distinct negative one at 209 nm (Fig. 3A). Furthermore, a very weak band can be seen around 220 nm in this CD-spectrum. Results from deconvolution of the E2$_{dithiol}$ CD-spectrum are listed in Table SIII and a calculated spectrum is displayed in Fig. 3B. Results from analysis of E2$_{dithiol}$ using CONTIN L suggest that E2$_{dithiol}$ has an α-helical content around 80 %. Because the normalized root mean square deviation (NMRSD) is very high (0.3) for the deconvolution of the CD-spectrum for E2$_{dithiol}$, the calculated secondary structure is probably not going to be in complete agreement with the actual one.[53] However, both the experimental and calculated spectra clearly indicate the presence of some α-helical structure in E2$_{dithiol}$. Deconvolution of the E2$_{disulfide}$ spectrum suggests α-helical content close to 60 % (Table IV). It should be noted that CONTIN L also predicts the presence of a turn (43 %) in this peptide. Again the NMRSD-value is very high so no conclusions can be made about the ‘correct’ amount of α-helix in E2$_{disulfide}$. The experimental spectrum (Fig. 3A) features two of the bands indicative of α-helix (196 and 209 nm). The 222 nm band cannot be seen in the experimental or calculated spectra (Figs. 3A and 3B). However, because the E2$_{disulfide}$ spectrum has some of the bands typical of α-helix, the presence of α-helix cannot be ruled out in this case. In addition, the presence of some α-helix is supported, but not proven, by deconvolution of the E2$_{dithiol}$ CD spectrum.

Aromatic stacking

Due to the importance of aromatic stacking for stabilizing the receptor bundle structure in IMPs,[58] we examined the pattern of aromatic stacking in both CB$_1$(E2$_{dithiol}$) and

$CB_1(E2_{disulfide})$. As shown in Fig. 4A, a significant amount of receptor aromatic stacking occurs in the membrane region between −20 and +30 Å along the Z-axis. An extensive aromatic stacking network exists in the region between +5 and +15 Å, centering at $W356^{6.48}$: $F170^{2.57}$/$W356^{6.48}$/$F200^{3.36}$/$F278^{5.42}$($W279^{5.43}$)/$Y275^{5.39}$ in both $CB_1(E2_{dithiol})$ and $CB_1(E2_{disulfide})$.

The number of aromatic stacking interactions in the extracellular top layer around +20 Å is maintained low in $CB_1(E2_{dithiol})$, yet gradually increased in $CB_1(E2_{disulfide})$ as the simulation continues (Fig. 4A). A detailed examination reveals that in this region the aromatic stacking network by $F268^{E2}$/$H270^{E2}$/$Y275^{5.39}$ is well maintained only in $CB_1(E2_{disulfide})$ but is unavailable in $CB_1(E2_{dithiol})$ due to the location of $H270^{E2}$: $H270^{E2}$ in $CB_1(E2_{dithiol})$, exposed to water, is not able to form aromatic stacking to $Y275^{5.39}$, while $H270^{E2}$ in $CB_1(E2_{disulfide})$, positioned toward the helical inner core region, forms aromatic stacking to $Y275^{5.39}$ and tightly connects the aromatic stacking network centered at $F268^{E2}$ in the extracellular region to the aromatic stacking network centered at $W356^{6.48}$ in the helical inner core region (Fig. 4B). Overall, the aromatic stacking at the extracellular region is better developed in $CB_1(E2_{disulfide})$ than in $CB_1(E2_{dithiol})$ due to distinct E2 structures.

Toggle switch $W356^{6.48}$

$W356^{6.48}$ of the CB_1 receptor has been proposed as a toggle switch for receptor activation,[62] similar to $W286^{6.48}$ of β_2AR.[63] The X-ray structure of rhodopsin[14] reveals that $W265^{6.48}$ is stabilized by aromatic stacking to $F261^{6.44}$ and $Y268^{6.51}$, highly homologous residues in many GPCRs.[64] The CB_1 receptor, however, lacks the corresponding aromatic residues at the 6.44 and 6.51 positions and, consequently, is expected to have unique interaction patterns for $W356^{6.48}$.

As shown in Fig. 4B, $F170^{2.57}$ and $F200^{3.36}$ of the CB_1 receptor form aromatic stacking to $W356^{6.48}$, suggesting their role in stabilizing $W356^{6.48}$. To gain insight into how $F170^{2.57}$ and $F200^{3.36}$ stabilize $W356^{6.48}$ in $CB_1(E2_{dithiol})$ and $CB_1(E2_{disulfide})$, the χ1 and χ2 angles of $F170^{2.57}$, $F200^{3.36}$ and $W356^{6.48}$ are analyzed (Fig. 4C). Closely surrounded by the neighboring residues, the aromatic ring of $F170^{2.57}$ appears to be rather fixed, with the χ1 and χ2 angles of $F170^{2.57}$ showing little change throughout the simulations of both $CB_1(E2_{dithiol})$ and $CB_1(E2_{disulfide})$. Of interest, it appears that the preferred value for the χ1 angle of $F200^{3.36}$ is ~ +180 degrees, common to both $CB_1(E2_{dithiol})$ and $CB_1(E2_{disulfide})$. In $CB_1(E2_{dithiol})$, as the χ1 angle of $F200^{3.36}$ changes to ~ +180 degrees early in the simulation, the χ1 angle of $W356^{6.48}$ maintains at ~ −70 degrees. In $CB_1(E2_{disulfide})$, however, as the χ1 angle of $F200^{3.36}$ changes to ~ +180 degrees late in the simulation, the χ1 angle of $W356^{6.48}$ changes from ~ −70 degrees to ~ −150 degrees. A close examination reveals that $F200^{3.36}$ in $CB_1(E2_{dithiol})$, flexible without any steric conflict with $W356^{6.48}$, achieves its preferred χ1 angle without any modification in the χ1 angle of $W356^{6.48}$, while $F200^{3.36}$ in $CB_1(E2_{disulfide})$, restricted in motion by $W356^{6.48}$, achieves its preferred χ1 angle with a significant modification in the χ1 angle of $W356^{6.48}$. As a result, the χ1 angle of $W356^{6.48}$ in $CB_1(E2_{dithiol})$ becomes ~ −70 degrees, indicative of the receptor in its inactive state[63], while the χ1 angle of $W356^{6.48}$ in $CB_1(E2_{disulfide})$ becomes ~ −150 degrees, indicative of the receptor in its active-like state[63]. Overall, differences in the χ1 angle of $W356^{6.48}$ shown in $CB_1(E2_{dithiol})$ and $CB_1(E2_{disulfide})$ indicate distinct E2 structures play a role in modulating the receptor conformational change required for its activation.[65]

Interaction energy analysis

To examine how distinct E2 structures exhibit different degrees of receptor stabilization, the inter-molecular interaction energy between E2 and the rest of the receptor ($E_{inter,E2}$) were estimated (Fig. 5A and Table SII). $E_{inter,E2}$ is −147.0 kcal/mol for $CB_1(E2_{dithiol})$ (i.e.,

−104.6 kcal/mol by TMH; −13.5 kcal/mol by E1; and −28.9 kcal/mol by E3), compared with −252.9 kcal/mol for $CB_1(E2_{disulfide})$ (i.e., −226.0 kcal/mol by TMH; −22.5 kcal/mol by E1; and −4.1 kcal/mol by E3), indicating that the receptor is more stabilized by E2 in $CB_1(E2_{disulfide})$ than E2 in $CB_1(E2_{dithiol})$. E2 in $CB_1(E2_{disulfide})$, with one helical turn, interacts more closely with TMH than E2 in $CB_1(E2_{dithiol})$, with two helical turns, possibly due to its flexibility that allows to be closely packed to TMH. In support, only in $CB_1(E2_{disulfide})$ but not in $CB_1(E2_{dithiol})$, the C-terminal residue $P269^{E2}$ forms a tight hydrophobic cluster with some residues from H3 and H4 as described above. E2 interacts favorably with E3 in $CB_1(E2_{dithiol})$ due to the salt bridge by $D266^{E2}/K370^{E3}$, which is absent in $CB_1(E2_{disulfide})$, and E2 interacts favorably with E1 in $CB_1(E2_{disulfide})$ due to the salt bridge by $K183^{E1}/D266^{E2}$, which is absent in $CB_1(E2_{dithiol})$. Overall, distinct E2 structures interact differently with the TM helical bundle as well as E1/E3.

Contact number analysis

To examine how distinct E2 structures modify the TM helical topology, the contact numbers were counted (Figs. 5B and 5C and Table SII). These contact numbers include not only those between E2 and the rest of the receptor but also the inter-helical contacts. The E2/TMH contact number is higher in $CB_1(E2_{disulfide})$ than in $CB_1(E2_{dithiol})$, which is also reflected in the E2/TMH interaction energies. The E2/E3 contact number is higher in $CB_1(E2_{dithiol})$ than in $CB_1(E2_{disulfide})$, which is also reflected in their E2/E3 interaction energies. Of interest, the E2/E1 contact number is almost identical in both $CB_1(E2_{dithiol})$ and $CB_1(E2_{disulfide})$, but the E2/E1 interaction energy is lower in $CB_1(E2_{disulfide})$ than in $CB_1(E2_{dithiol})$, due to the salt bridge by $K183^{E1}/D266^{E2}$ in $CB_1(E2_{disulfide})$.

Because most of TMH are not exactly perpendicular to the membrane, the TM helical topology at the extracellular region is different from that at the intracellular region. Thus, the inter-helical contact numbers are analyzed by considering two separate parts: the extacellular half and the intracellular half. As shown in Fig. 5C and Table SII, the high inter-helical contact numbers shown for H2/H7 on the extracellular side and for H1/H2 and H3/H5 on the intracellular side are in agreement with the notion that the TM helical bundle of the CB_1 receptor is primarily stabilized by H1/H2, H2/H7 and H3/H5.[32]

To examine the role of distinct E2 structures in TM helical rearrangement, the predicted TM helical structures in $CB_1(E2_{dithiol})$ and $CB_1(E2_{disulfide})$ suggested by the contact number analysis are compared with TMH in the CB_1 receptor model[32] (Fig. 5D) the template structure before the long simulation. For $CB_1(E2_{dithiol})$, H4/H5 move in toward the core and H1/H6/H7 move out of the core on the extracellular side, while H7 moves out of the core and H4/H5/H6 move toward the core on the intracellular side (Figs. 5Di & 5Diii). For $CB_1(E2_{disulfide})$, H4/H6 moves in toward the core and H1/H2/H5 move out of the core on the extracellular side, while H4/H6 moves into the core and H5 moves out of the core on the intracellular side (Figs. 5Dii & 5Div). Overall, the contact number analysis reveals that distinct E2 structures, with different degrees of molecular interaction with the rest of the receptor, induce unique alterations in the TM helical topology.

Core crevice analysis

Since the distinct E2 structures interact differently with the receptor bundle and uniquely alter the TM helical topology, we performed a core crevice analysis to examine key differences in the binding pockets in $CB_1(E2_{dithiol})$ and $CB_1(E2_{disulfide})$. As shown in Fig. 6A, common to both $CB_1(E2_{dithiol})$ and $CB_1(E2_{disulfide})$, the core crevice is almost completely closed at the inner core region between −10 Å and +10 Å along the Z-axis. In contrast, in the extracellular region between +10 Å and +20 Å, the water molecules are able to enter into the ligand binding core crevice. A close examination reveals that in

$CB_1(E2_{dithiol})$, E2, positioned near the extracellular ends of H3/H4/H5, occupies only half of the extracellular pore, leaving the extracellular pore formed by H2/H3/H7 accessible to water. The binding core crevice in $CB_1(E2_{dithiol})$ with the predicted crevice diameters of > 6 Å appears to be fully developed to include the region deep in the binding pocket (Fig. 6Bi). Similarly, E2 in $CB_1(E2_{disulfide})$, positioned over H3/H4, leaves the extracellular pore region formed by H2/H3/H7 relatively open to water access. However, the predicted crevice diameters of ≤ 6 Å in $CB_1(E2_{disulfide})$ appear to restrict ligand access to the binding pocket (Fig. 6Bii). Differences in core crevice of $CB_1(E2_{dithiol})$ and $CB_1(E2_{disulfide})$ demonstrate the topologically distinct rearrangement of TMH initiated by distinct E2 structures, suggesting the role of E2 not only in the availability but also the dimensions of the ligand binding pore.

Cross-correlation analysis

To gain some insights into the role of distinct E2 structures in unique modifications in the TM helical topology, we also performed cross-correlation analysis for $CB_1(E2_{dithiol})$ and $CB_1(E2_{disulfide})$. The pattern of correlation of $CB_1(E2_{dithiol})$ quite differs from that of $CB_1(E2_{disulfide})$ (Fig. 7): only limited TMH, including H2, H5 and H6, are correlated in $CB_1(E2_{dithiol})$, while most of TMH are correlated in $CB_1(E2_{disulfide})$. Common to both $CB_1(E2_{dithiol})$ and $CB_1(E2_{disulfide})$, the N-terminal region of E2, containing the helical segment, is not involved in coupling. In contrast, the C-terminal region of E2 in $CB_1(E2_{dithiol})$ is coupled to H5, while the same region in $CB_1(E2_{disulfide})$ is coupled not only to most of TM helices but also to E1 and E3. Of interest, the segment spanning from the E2 C-terminal region to the N-terminal region of I3 in $CB_1(E2_{disulfide})$ appears to be closely coupled together, possibly due to H5 fluctuation initiated by E2 fluctuation (Fig. 2Ai), as indicated by the moderate E2/H5 coupling (Fig. 7ii). Overall, these results strongly suggest that distinct E2 structures are uniquely coupled to the TM helical bundle to modify TM helical topology.

DISCUSSION

The presence of a helical segment within E2 both in $CB_1(E2_{dithiol})$ (i.e., $C257^{E2}$-$V263^{E2}$) and in $CB_1(E2_{disulfide})$ (i.e., $C257^{E2}$-$L260^{E2}$), as seen in the X-ray structures of βARs[15,16] and as predicted by several popular secondary prediction programs (Table I), is strongly suggested by the CD spectra of two E2 peptides (Fig. 3). It appears that the E2 helical segment in an amphipathic alignment, located in the membrane-water interfacial region, plays a role in stabilizing receptor structure. Furthermore, it appears that the degree of the helical content determines the flexibility of E2, which is important for its interaction with TMH (see below).

It has been reported that GPCR E2 plays an important role in receptor activation,[65] primarily by coupling to the TM helical domain.[13,66,67] The present study strongly suggests that E2 of the CB_1 receptor is able to rearrange TMH through E2/TMH coupling. Examining the degree of E2 interaction with TMH in $CB_1(E2_{dithiol})$ and $CB_1(E2_{disulfide})$, we demonstrate that distinct E2 structures of the CB_1 receptor uniquely modify the TM helical topology. The strong coupling between E2 and TMH observed in $CB_1(E2_{disulfide})$ (Fig. 7ii) appears to be attributed to the flexible nature of E2, which allows the C-terminal region of E2 to be inserted into the extracellular H3/H5 region for close interactions with the extracellular end residues of TMH: 1) the hydrophobic packing by $P269^{E2}$ to the TM hydrophobic residues $L190^{3.26}$, $L193^{3.29}$ and $L253^{4.62}$; and/or 2) the aromatic stacking centering at $F268^{E2}$/$H270^{E2}$/$Y275^{5.39}$. As a result, H5 moves out from H3 and at the same time H6 moves in toward H3 at the extracellular region (Fig. 5Dii). These helical movements are evidenced by TMH/E3 fluctuation caused by E2 fluctuation (Fig. 2Aii). As demonstrated in a recent NMR study[61], the outward movement of H5 and the inward movement of H6 at the extracellular

region appear to be necessary for an efficient coupling of E2 to TMH. Conversely, in $CB_1(E2_{dithiol})$, E2 with the much reduced flexibility is less inserted into the extracellular H3/H5 region. As a result, H5 moves in toward H3 and at the same time H6 moves away from H3 at the extracellular region (Fig. 5Di). Thus, it appears that the E2 C-terminal residues determine the E2 conformation, which is important for its coupling to TMH and thereby for receptor activation. The importance of the E2 C-terminal region for the CB_1 receptor activation has been suggested by a recent study by Ahn et al.[61] where the Ala mutations of the C-terminal residues of E2 in the CB_1 receptor significantly reduced the agonist binding but retained the inverse agonist binding. It appears that the C-terminal residues of E2 not only provide the binding contact sites exclusively for agonist binding but also initiate the conformational change in TMH required for receptor activation. It should be noted that although the coupling between E2 and TMH expects to be weak in the absence of the ligand, E2 conformational rearrangement upon ligand binding, as demonstrated in several experimental studies of other GPCRs,[18,19,68] and the subsequent coupling to TMH, especially the segments of H5, are presumed to induce a ligand-specific conformational change in the CB_1 receptor.

Considering that the CB_1 receptor binding pocket consists of the TM helical core residues at the extracellular region mainly from H3/H5/H6/H7,[69,70] the outward movement of H6 from the core and the inward movement of H5 in $CB_1(E2_{dithiol})$ and the outward movement of H5 and the inward movement of H6 in $CB_1(E2_{disulfide})$ (Fig. 5D) would uniquely modify the ligand binding pocket located in the extracellular core region of the receptor (Fig. 6B). It is known for the CB_1 receptor that $F189^{3.25}$, $W255^{4.64}$, $F268^{E2}$ and $Y275^{5.39}$ are crucial for agonist recognition.[56,60,61] Since the aromatic stacking networks by $F189^{3.25}/F268^{E2}$ connected to $Y275^{5.39}$ are only available for $CB_1(E2_{disulfide})$ (Fig. 4B), $CB_1(E2_{disulfide})$ appears to be more suitable than $CB_1(E2_{dithiol})$ in maintaining the agonist binding pocket geometry. Similarly, it has been suggested that antagonist binding is more sensitive than agonist binding to the cleavage of the E2 disulfide bond of the CB_1 receptor.[21] Thus, $CB_1(E2_{disulfide})$ appears to be more suitable than $CB_1(E2_{dithiol})$ in maintaining the antagonist binding pocket geometry. Thus, it is conceivable that the outward movement of H5 and the inward movement of H6 at the extracellular region shown in $CB_1(E2_{disulfide})$ is beneficial to ligand binding, while the outward movement of H6 and the inward movement of H5 at the extracellular region shown in $CB_1(E2_{dithiol})$ is detrimental to ligand binding. Considering that I3, which connects H5 and H6 and forms one of the main interfaces to the coupled G-protein, is crucial for transferring the molecular signal from ligand binding at the extracellular face during receptor activation,[71] the inward movement of H5 and H6 in $CB_1(E2_{dithiol})$ and the outward movement of H5 and the inward movement of H6 in $CB_1(E2_{disulfide})$ at the intracellular region would lead to distinct I3 conformations as E2 conformation-specific molecular signals.

In the present study, $CB_1(E2_{disulfide})$ appears to be more biologically relevant than $CB_1(E2_{dithiol})$. One of the main reasons for the preference of $CB_1(E2_{disulfide})$ over $CB_1(E2_{dithiol})$ is that $CB_1(E2_{disulfide})$ contains an extensive aromatic stacking network covering the region between +5 Å and +20 Å, while $CB_1(E2_{dithiol})$ lacks such aromatic stacking (Fig. 4B). It appears that the aromatic residues in this region not only contribute to stabilizing the ligand binding pocket through aromatic stacking but also serve as the initial ligand contact site at the extracellular top surface of the receptor. It appears that the aromatic stacking network centered at $F189^{3.25}$ and $F268^{E2}$ in the extracellular region at the entrance of the ligand binding pocket plays a role as a gate keeper, selectively allowing the right type of ligand to enter into the binding pocket region (Fig. 6B). Thus, upon ligand entry the aromatic cluster is rearranged in such a way that the entrance of the binding pocket is opened for ligand access. It is interesting to note that $CB_1(E2_{dithiol})$ represents a gate-open form as the aromatic stacking by $F189^{3.25}/F268^{E2}$ is absent, while $CB_1(E2_{disulfide})$

represents a gate-closed form as the aromatic stacking by $F189^{3.25}$/$F268^{E2}$ is present. Similarly, a recent study of β_2AR suggests that the E2/H7 hydrophobic junction of the ligand-free receptor is partially broken upon ligand entry, while the hydrophobic cleft formed by H2/H3/H7 serves as a specific ligand-entry site.[72] It appears that the binding core crevice shown in the present receptor models (Fig. 6) are strongly supported by experimental findings[30,60,61,73] of key residues shaping the ligand binding pocket: for the extracellular part, $F268^{E2}$ and $F189^{3.25}$; for the middle part, $I362^{6.54}$ and $M363^{6.55}$; and for the inner core part, $Y275^{5.39}$, $L359^{6.51}$ and $L360^{6.52}$.

Another key reason for the preference of $CB_1(E2_{disulfide})$ over $CB_1(E2_{dithiol})$ is that $CB_1(E2_{disulfide})$ contains the disulfide bond in E2, while $CB_1(E2_{dithiol})$ does not. An early ligand binding study by Martin and his colleagues[31] showed that dithiothreitol (DTT), a disulfide reducing agent, decreased the binding affinity of CP55940 by ~ 50 % regardless of the pretreatment of CP55940 to protect the binding site, indicating that a disulfide bond that affects CP55940 binding "exists" and such disulfide bond is not located at the CP55940 binding pocket. In $CB_1(E2_{disulfide})$, the E2 disulfide bond is located in the extracellular top region (Fig. 6Bii) off the CP55940 binding pocket and exposed to solvent, indicating that the disulfide bond is easily accessible to DTT for reduction. In contrast, in $CB_1(E2_{dithiol})$ the only residues that are somewhat close to form a disulfide bond are $C355^{6.47}$ and $C386^{7.42}$. However, the formation of the disulfide bond by these Cys residues appears to contradict the experimental results suggesting that the disulfide bond is not located at the CP55940 binding pocket,[31] for $C355^{6.47}$ is known to be a binding pocket residue.74 From the above-mentioned ligand binding study,[31] it was also shown that sulfhydryl blocking agents (SBAs) decreased the binding affinity of CP55940 by > 90 % but significantly reduced the decrease in CP55940 binding (< 50 %) by the pretreatment of CP55940. These results suggest that a reactive free thiol of the receptor exists near or at the CP55940 ligand binding site. The Cys residues located near the CP55940 binding site include $C355^{6.47}$ and $C386^{7.42}$ at the helical core. Among these Cys residues, $C355^{6.47}$ would be a better candidate than $C386^{7.42}$ in providing the reactive free thiol to SBAs for the following reasons: 1) $C355^{6.47}$ is known to form part of the CP55940 binding site;[74] and 2) it is known that the sulfhydryl blocking of $C386^{7.42}$ did not affect CP55940 binding.[21]

As shown in Fig. 8, the experimental results reported by Martin and his colleagues[31] can be explained as follows: the observed ~ 50 % decrease in CP55940 binding affinity, regardless of the pretreatment of CP55940, by DTT (i.e., the reduction of the disulfide bond) is less likely to be due to the direct modification of the binding pocket but rather indirect modification as the E2 disulfide bond is reduced. Such indirect modification of the binding pocket is indicated by the results of the present study demonstrating that distinct E2 structures are able to modify the TM helical topology through the E2/H5 coupling (Fig. 7). As discussed before, $CB_1(E2_{disulfide})$, which is equivalent to the receptor before DTT reduction, is more suitable than $CB_1(E2_{dithiol})$, which is equivalent to the receptor after DTT reduction, in maintaining the agonist binding pocket geometry. It should be noted that the protection of the ligand binding pocket by the pretreatment of the ligand does not prevent the ligand binding pocket from the modification caused by the reduction of the E2 Cys disulfide bond (Fig. 8A), indicating that the impact of E2 structural change on the receptor TM helical bundle is rather significant. In contrast, the finding that the decrease in CP55940 binding by SBAs was significantly reduced by the pretreatment of CP55940 is due to the protection of the binding pocket by CP55940 that prevents the modification of the binding pocket by SBAs, leading to a significant reduction of the decrease in CP55940 binding (Fig. 8B).

It is very intriguing to see that $CB_1(E2_{disulfide})$ is converted to an active-like state, while $CB_1(E2_{dithiol})$ maintains the inactive state, as judged from the the $\chi 1$ angle of $W356^{6.48}$.[63]

The flipping of the indole ring of $W356^{6.48}$ (i.e., the χ1 angle = ~ −150 degrees) occurs at the late stage of the simulation and is maintained for the rest of the simulation, indicating the resulting structure is somewhat stable in spite of the continued fluctuation. It should be noted, however, that the salt bridge between $R214^{3.50}$ and $D338^{6.30}$, which has been proposed as the ionic lock[75] for the corresponding residues $R131^{3.50}$ and $E268^{6.30}$ in β_2AR that retains the receptor in the inactive state, is maintained in $CB_1(E2_{disulfide})$, suggesting that $CB_1(E2_{disulfide})$ resembles the receptor in its inactive state but possibly at the early intermediate stage of the active state. Comparison of $CB_1(E2_{dithiol})$ with $CB_1(E2_{disulfide})$ suggests that the $W356^{6.48}$ ring flipping in $CB_1(E2_{disulfide})$ occurs due to the steric conflict between $W356^{6.48}$ and $F200^{3.36}$ caused by the inward movement of H6 toward H3 at the extracellular region (Figure 5Dii). Thus, it is possible that one of the key steps at the early stage of receptor activation involves the initial ligand binding to the E2 C-terminal (aromatic) residues[61] and the subsequent rearrangement of TMH, H5 and H6 in particular, through E2 coupling, leading to the turning on of the toggle switch $W356^{6.48}$ (i.e., the ring flipping).[62] It should be noted that $W356^{6.48}$ and $F200^{3.36}$ are known to be important for ligand binding and receptor function.[60,61,73,76] The proposed receptor activation by the direct coupling between E2 and the TM helical bundle[13,66,67] is applicable to the CB_1 receptor, as demonstrated by the present correlation analysis (Fig. 7). Further study of the TM helical bundle of the CB_1 receptor may provide insight into the molecular mechanism of the receptor activation initiated by $W356^{6.48}$, the residue proposed as a toggle switch in the CB_1 receptor.[62]

CONCLUSION

In the present study, two alternative forms, $E2_{dithiol}$ and $E2_{disulfide}$, are considered as distinct E2 structures of the CB_1 receptor. It is demonstrated that the CB_1 receptor can have an α-helical segment within E2, as predicted by several secondary structure prediction programs and similar to βARs,[15,16] which remains stable in the membrane-water interfacial region. It is also demonstrated that different TM helical topologies, including the binding pocket crevice at the extracellular region and the receptor interface to the coupled G-protein at the intracellular region, are induced by distinct E2 structures through the direct coupling between E2 and TMH. The present results suggest the critical role of the CB_1 E2 in stabilizing the receptor, regulating ligand binding through modification of the binding pocket, and ultimately modulating receptor activation, as shown in other GPCRs.[5–7,13,65,77] Further studies on the role of E2 of the CB_1 receptor are warranted; particularly comparisons of the ligand-bound form with the present ligand-free form.

Supplementary Material

Refer to Web version on PubMed Central for supplementary material.

Acknowledgments

This work was partially supported by the NIDA K01-DA020663 & by the NCSA under MCB080037N and utilized the Teragrid BigRed IBM e1350 (Indiana University) and LoneStar Dell PowerEdge 1955 (The University of Texas at Austin). The authors thank Drs. L. Pedersen and L. Perera for many helpful discussions. The authors also thank Dr. S. Shaikh for assisting of the g_correlation analysis.

REFERENCES

1. Matsuda LA, Lolait SJ, Brownstein MJ, Young AC, Bonner TI. Structure of a cannabinoid receptor and functional expression of the cloned cDNA. Nature. 1990; 346:561–564. [PubMed: 2165569]
2. Gether U. Uncovering molecular mechanisms involved in activation of G protein-coupled receptors. Endocr Rev. 2000; 21:90–113. [PubMed: 10696571]

3. Elofsson A, von Heijne G. Membrane protein structure: prediction versus reality. Annu Rev Biochem. 2007; 76:125–140. [PubMed: 17579561]
4. Bowie JU. Solving the membrane protein folding problem. Nature. 2005; 438:581–589. [PubMed: 16319877]
5. Marti T. Refolding of bacteriorhodopsin from expressed polypeptide fragments. J Biol Chem. 1998; 273:9312–9322. [PubMed: 9535926]
6. de Planque MR, Kruijtzer JA, Liskamp RM, Marsh D, Greathouse DV, Koeppe RE 2nd, de Kruijff B, Killian JA. Different membrane anchoring positions of tryptophan and lysine in synthetic transmembrane alpha-helical peptides. J Biol Chem. 1999; 274:20839–20846. [PubMed: 10409625]
7. Klco JM, Wiegand CB, Narzinski K, Baranski TJ. Essential role for the second extracellular loop in C5a receptor activation. Nat Struct Mol Biol. 2005; 12:320–326. [PubMed: 15768031]
8. Ulmschneider MB, Tieleman DP, Sansom MS. The role of extra-membranous inter-helical loops in helix-helix interactions. Protein Eng Des Sel. 2005; 18:563–570. [PubMed: 16251222]
9. Ji TH, Grossmann M, Ji I. G protein-coupled receptors I Diversity of receptor-ligand interactions. J Biol Chem. 1998; 273:17299–17302. [PubMed: 9651309]
10. Shi L, Javitch JA. The second extracellular loop of the dopamine D2 receptor lines the binding-site crevice. Proc Natl Acad Sci USA. 2004; 101:440–445. [PubMed: 14704269]
11. Scarselli M, Li B, Kim SK, Wess J. Multiple residues in the second extracellular loop are critical for M3 muscarinic acetylcholine receptor activation. J Biol Chem. 2007; 282:7385–7396. [PubMed: 17213190]
12. Avlani VA, Gregory KJ, Morton CJ, Parker MW, Sexton PM, Christopoulos A. Critical role for the second extracellular loop in the binding of both orthosteric and allosteric G protein-coupled receptor ligands. J Biol Chem. 2007; 282:25677–25686. [PubMed: 17591774]
13. Ahuja S, Hornak V, Yan EC, Syrett N, Goncalves JA, Hirshfeld A, Ziliox M, Sakmar TP, Sheves M, Reeves PJ, Smith SO, Eilers M. Helix movement is coupled to displacement of the second extracellular loop in rhodopsin activation. Nat Struct Mol Biol. 2009; 16:168–175. [PubMed: 19182802]
14. Okada T, Sugihara M, Bondar AN, Elstner M, Entel P, Buss V. The retinal conformation and its environment in rhodopsin in light of a new 2.2 Å crystal structure. J Mol Biol. 2004; 342:571–583. [PubMed: 15327956]
15. Cherezov V, Rosenbaum DM, Hanson MA, Rasmussen SG, Thian FS, Kobilka TS, Choi HJ, Kuhn P, Weis WI, Kobilka BK, Stevens RC. High-resolution crystal structure of an engineered human beta2-adrenergic G protein-coupled receptor. Science. 2007; 318:1258–1265. [PubMed: 17962520]
16. Warne T, Serrano-Vega MJ, Baker JG, Moukhametzianov R, Edwards PC, Henderson R, Leslie AG, Tate CG, Schertler GF. Structure of a beta1-adrenergic G-protein-coupled receptor. Nature. 2008; 454:486–491. [PubMed: 18594507]
17. Jaakola VP, Griffith MT, Hanson MA, Cherezov V, Chien EY, Lane JR, Ijzerman AP, Stevens RC. The 2.6 angstrom crystal structure of a human A2A adenosine receptor bound to an antagonist. Science. 2008; 322:1211–1217. [PubMed: 18832607]
18. Banères JL, Mesnier D, Martin A, Joubert L, Dumuis A, Bockaert J. Molecular characterization of a purified 5-HT4 receptor: a structural basis for drug efficacy. J Biol Chem. 2005; 280:20253–20260. [PubMed: 15774473]
19. Khasawneh FT, Huang JS, Turek JW, Le Breton GC. Differential mapping of the amino acids mediating agonist and antagonist coordination with the human thromboxane A2 receptor protein. J Biol Chem. 2006; 281:26951–26965. [PubMed: 16837469]
20. Shire D, Calandra B, Delpech M, Dumont X, Kaghad M, Le Fur G, Caput D, Ferrara P. Structural features of the central cannabinoid CB1 receptor involved in the binding of the specific CB1 antagonist SR 141716A. J Biol Chem. 1996; 271:6941–6946. [PubMed: 8636122]
21. Fay JF, Dunham TD, Farrens DL. Cysteine residues in the human cannabinoid receptor: only C257 and C264 are required for a functional receptor, and steric bulk at C386 impairs antagonist SR141716A binding. Biochemistry. 2005; 44:8757–8769. [PubMed: 15952782]
22. de Bakker PI, DePristo MA, Burke DF, Blundell TL. Ab initio construction of polypeptide fragments: Accuracy of loop decoy discrimination by an all-atom statistical potential and the

AMBER force field with the Generalized Born solvation model. Proteins. 2003; 51:21–40. [PubMed: 12596261]

23. McGuffin LJ, Bryson K, Jones DT. The PSIPRED protein structure prediction server. Bioinformatics. 2000; 16:404–405. [PubMed: 10869041]
24. Cole C, Barber JD, Barton J. The Jpred 3 secondary structure prediction server. Nucleic Acids Res. 2008; 36:W197–W201. [PubMed: 18463136]
25. Raghava GPS. Protein secondary structure prediction using nearest neighbor and neural network approach. CASP4. 2000:75–76.
26. Karnik SS, Sakmar TP, Chen HB, Khorana HG. Cysteine residues 110 and 187 are essential for the formation of correct structure in bovine rhodopsin. Proc Natl Acad Sci USA. 1988; 85:8459–8463. [PubMed: 3186735]
27. Davidson FF, Loewen PC, Khorana HG. Structure and function in rhodopsin: replacement by alanine of cysteine residues 110 and 187, components of a conserved disulfide bond in rhodopsin, affects the light-activated metarhodopsin II state. Proc Natl Acad Sci USA. 1994; 91:4029–4033. [PubMed: 8171030]
28. Hwa J, Klein-Seetharaman J, Khorana HG. Structure and function in rhodopsin: Mass spectrometric identification of the abnormal intradiscal disulfide bond in misfolded retinitis pigmentosa mutants. Proc Natl Acad Sci USA. 2001; 98:4872–4876. [PubMed: 11320236]
29. Karnik SS, Gogonea C, Patil S, Saad Y, Takezako T. Activation of G-protein-coupled receptors: a common molecular mechanism. Trends Endocrinol Metab. 2003; 14:431–437. [PubMed: 14580763]
30. Nebane NM, Hurst DP, Carrasquer CA, Qiao Z, Reggio PH, Song ZH. Residues accessible in the binding-site crevice of transmembrane helix 6 of the CB2 cannabinoid receptor. Biochemistry. 2008; 47:13811–13821. [PubMed: 19053233]
31. Lu R, Hubbard JR, Martin BR, Kalimi MY. Roles of sulfhydryl and disulfide groups in the binding of CP-55,940 to rat brain cannabinoid receptor. Mol Cell Biochem. 1993; 121:119–126. [PubMed: 8316228]
32. Shim J-Y. The transmembrane helical domain of the cannabinoid CB_1 receptor. Biophys J. 2009; 96:3251–3262. [PubMed: 19383469]
33. Ballesteros, JA.; Weinstein, H. Integrated methods for modeling G-protein coupled receptors. In: PM, Conn; SC, Sealfon, editors. Methods in Neuroscience. San Francisco: Academic Press; 1995. p. 366-428.
34. Phillips JC, Braun R, Wang W, Gumbart J, Tajkhorshid E, Villa E, Chipot C, Skeel RD, Kalé L, Schulten K. Scalable molecular dynamics with NAMD. J Comput Chem. 2005; 26:1781–1802. [PubMed: 16222654]
35. Chen J, Im W, Brooks CL 3rd. Balancing solvation and intramolecular interactions: toward a consistent generalized Born force field. J Am Chem Soc. 2006; 128:3728–3736. [PubMed: 16536547]
36. Buck M, Bouguet-Bonnet S, Pastor RW, MacKerell AD Jr. Importance of the CMAP correction to the CHARMM22 protein force field: dynamics of hen lysozyme. Biophys J. 2006; 90:L36–L38. [PubMed: 16361340]
37. Brooks BR, Bruccoleri RE, Olafson BD, States DJ, Swaminathan S, Karplus M. CHARMM: A Program for Macromolecular Energy Minimization, and Dynamics Calculations. J Comp Chem. 1983; 4:187–217.
38. MacKerell AD Jr, Bashford D, Bellott M, Dunbrack RL Jr, Evanseck J, Field MJ, Fischer S, Gao J, Guo H, Ha S, Joseph D, Kuchnir L, Kuczera K, Lau FTK, Mattos C, Michnick S, Ngo T, Nguyen DT, Prodhom B, Reiher IWE, Roux B, Schlenkrich M, Smith J, Stote R, Straub J, Watanabe M, Wiorkiewicz-Kuczera J, Yin D, Karplus M. All-atom empirical potential for molecular modeling and dynamics studies of proteins. J Phys Chem B. 1998; 102:3586–3616.
39. Feller S, MacKerell AD Jr. An Improved Empirical Potential Energy Function for Molecular Simulations of Phospholipids. J Phys Chem B. 2000; 104:7510–7515.
40. Saam J, Tajkhorshid E, Hayashi S, Schulten K. Molecular dynamics investigation of primary photoinduced events in the activation of rhodopsin. Biophys J. 2002; 83:3097–3112. [PubMed: 12496081]

41. Feller SE, Zhang Y, Pastor RW, Brooks BR. Constant pressure molecular dynamics simulation: The Langevin piston method. J Chem Phys. 1995; 103:4613–4621.
42. Hoover WG. Canonical dynamics: Equilibrium phase-space distributions. Phys Rev A. 1985; 31:1695–1697. [PubMed: 9895674]
43. Essmann U, Perera L, Berkowitz ML, Darden T, Lee H, Pedersen LG. A smooth particle-mesh Ewald method. J Chem Phys. 1995; 103:8577–8593.
44. Tuckerman M, Berne BJ. Reversible multiple time scale molecular dynamics. J Chem Phys. 1992; 97:1990–2001.
45. Fiser A, Do RKG, Sali A. Modeling of loops in protein structures. Prot Sci. 2000; 9:1753–1773.
46. Darve E, Pohorille A. Calculating free energies using average force. J Chem Phys. 2001; 115:9169–9183.
47. Hénin J, Chipot C. Overcoming free energy barriers using unconstrained molecular dynamics simulations. J Chem Phys. 2004; 121:2904–2914. [PubMed: 15291601]
48. Hooft RW, Vriend G, Sander C, Abola EE. Errors in protein structures. Nature. 1996; 381:272. [PubMed: 8692262]
49. McGuffin LJ, Jones DT. Improvement of the GenTHREADER method for genomic fold recognition. Bioinformatics. 2003; 19:874–881. [PubMed: 12724298]
50. Gordon WR, Vardar-Ulu D, Histen G, Sanchez-Irizarry C, Aster JC, Blacklow SC. Structural basis for autoinhibition of Notch. Nat Struct Mol Biol. 2007; 14:295–300. [PubMed: 17401372]
51. Lange OF, Grubmüller H. Generalized Correlation for Biomolecular Dynamics. Proteins. 2006; 62:1053–1061. [PubMed: 16355416]
52. Smart OS, Goodfellow JM, Wallace BA. The Pore Dimensions of Gramicidin A. Biophys J. 1993; 65:2455–2460. [PubMed: 7508762]
53. Whitmore L, Wallace BA. DICHROWEB an online server for protein secondary structure analyses from circular dichroism spectroscopic data. Nucleic Acids Res. 2004; 32:W668–W673. Web Server issue. [PubMed: 15215473]
54. Chothia C. Structural invariants in protein folding. Nature. 1975; 254:304–308. [PubMed: 1118010]
55. Fersht, A. Structure and Mechanism in Protein Science. New York: W. H. Freeman and Company; 1999. p. 508-539.
56. Murphy JW, Kendall DA. Integrity of extracellular loop 1 of the human cannabinoid receptor 1 is critical for high-affinity binding of the ligand CP 55,940 but not SR 141716A. Biochem Pharmacol. 2003; 65:1623–1631. [PubMed: 12754098]
57. Kapur A, Samaniego P, Thakur GA, Makriyannis A, Abood ME. Mapping the structural requirements in the CB1 cannabinoid receptor transmembrane helix II for signal transduction. J Pharmacol Exp Ther. 2008; 325:341–348. [PubMed: 18174385]
58. Johnson RM, Hecht K, Deber CM. Aromatic and cation-pi interactions enhance helix-helix association in a membrane environment. Biochemistry. 2007; 46:9208–9214. [PubMed: 17658897]
59. Song ZH, Feng W. Absence of a conserved proline and presence of a conserved tyrosine in the CB2 cannabinoid receptor are crucial for its function. FEBS Lett. 2002; 531:290–294. [PubMed: 12417328]
60. McAllister SD, Rizvi G, Anavi-Goffer S, Hurst DP, Barnett-Norris J, Lynch DL, Reggio PH, Abood ME. An aromatic microdomain at the cannabinoid CB(1) receptor constitutes an agonist/inverse agonist binding region. J Med Chem. 2003; 46:5139–5152. [PubMed: 14613317]
61. Ahn KH, Bertalovitz AC, Mierke DF, Kendall DA. Dual Role of the Second Extracellular Loop of the Cannabinoid Receptor One: Ligand Binding and Receptor Localization. Mol Pharmacol. 2009; 76:833–842. [PubMed: 19643997]
62. Singh R, Hurst DP, Barnett-Norris J, Lynch DL, Reggio PH, Guarnieri F. Activation of the cannabinoid CB1 receptor may involve a W6 48/F3 36 rotamer toggle switch. J Pept Res. 2002; 60:357–370. [PubMed: 12464114]

63. Shi L, Liapakis G, Xu R, Guarnieri F, Ballesteros JA, Javitch JA. Beta2 adrenergic receptor activation Modulation of the proline kink in transmembrane 6 by a rotamer toggle switch. J Biol Chem. 2002; 277:40989–40996. [PubMed: 12167654]
64. Baldwin JM, Schertler GF, Unger VM. An alpha-carbon template for the transmembrane helices in the rhodopsin family of G-protein-coupled receptors. J Mol Biol. 1997; 272:144–164. [PubMed: 9299344]
65. Massotte D, Kieffer BL. The second extracellular loop: a damper for G protein-coupled receptors? Nat. Struct Mol Biol. 2005; 12:287–288.
66. Goodwin JA, Hulme EC, Langmead CJ, Tehan BG. Roof and floor of the muscarinic binding pocket: variations in the binding modes of orthosteric ligands. Mol Pharmacol. 2007; 72:1484–1496. [PubMed: 17848601]
67. Jäger D, Schmalenbach C, Prilla S, Schrobang J, Kebig A, Sennwitz M, Heller E, Tränkle C, Holzgrabe U, Höltje HD, Mohr K. Allosteric small molecules unveil a role of an extracellular E2/transmembrane helix 7 junction for G protein-coupled receptor activation. J Biol Chem. 2007; 282:34968–34976. [PubMed: 17890226]
68. Ruan KH, Cervantes V, Wu J. Ligand-specific conformation determines agonist activation and antagonist blockade in purified human thromboxane A2 receptor. Biochemistry. 2009; 48:3157–3165. [PubMed: 19170518]
69. Reggio PH. Ligand-ligand and ligand-receptor approaches to modeling the cannabinoid CB1 and CB2 receptors: achievements and challenges. Curr Med Chem. 1999; 6:665–683. [PubMed: 10469885]
70. Kapur A, Hurst DP, Fleischer D, Whitnell R, Thakur GA, Makriyannis A, Reggio PH, Abood ME. Mutation studies of Ser7.39 and Ser2.60 in the human CB1 cannabinoid receptor: evidence for a serine-induced bend in CB1 transmembrane helix 7. Mol Pharmacol. 2007; 71:1512–1524. [PubMed: 17384224]
71. Howlett, AC.; Padgett, LW.; Shim, J-Y. Cannabinoid agonist-selective regulation of G-protein coupling. In: PH, Reggio, editor. The Cannabinoid Receptors. New York: Humana Press; 2008. p. 173-193.
72. Wang T, Duan Y. Ligand entry and exit pathways in the beta2-adrenergic receptor. J Mol Biol. 2009; 392:1102–1115. [PubMed: 19665031]
73. McAllister SD, Tao Q, Barnett-Norris J, Buehner K, Hurst DP, Guarnieri F, Reggio PH, Nowell Harmon KW, Cabral GA, Abood ME. A critical role for a tyrosine residue in the cannabinoid receptors for ligand recognition. Biochem Pharmacol. 2002; 63:2121–2136. [PubMed: 12110371]
74. Picone RP, Khanolkar AD, Xu W, Ayotte LA, Thakur GA, Hurst DP, Abood ME, Reggio PH, Fournier DJ, Makriyannis A. (−)-7'-Isothiocyanato-11-hydroxy-1',1'-dimethylheptylhexahydrocannabinol (AM841), a high-affinity electrophilic ligand, interacts covalently with a cysteine in helix six and activates the CB1 cannabinoid receptor. Mol Pharmacol. 2005; 68:1623–1635. [PubMed: 16157695]
75. Ballesteros JA, Jensen AD, Liapakis G, Rasmussen SG, Shi L, Gether U, Javitch JA. Activation of the beta 2-adrenergic receptor involves disruption of an ionic lock between the cytoplasmic ends of transmembrane segments 3 and 6. J Biol Chem. 2001; 276:29171–29177. [PubMed: 11375997]
76. Shen CP, Xiao JC, Armstrong H, Hagmann W, Fong TM. F200A substitution in the third transmembrane helix of human cannabinoid CB1 receptor converts AM2233 from receptor agonist to inverse agonist. Eur J Pharmacol. 2006; 531:41–46. [PubMed: 16438957]
77. Tastan O, Klein-Seetharaman J, Meirovitch H. The effect of loops on the structural organization of alpha-helical membrane proteins. Biophys J. 2009; 96:2299–2312. [PubMed: 19289056]
78. Kabsch W, Sander C. Dictionary of protein secondary structure: pattern recognition of hydrogen-bonded and geometrical features. Biopolymers. 1983; 22:2577–2637. [PubMed: 6667333]

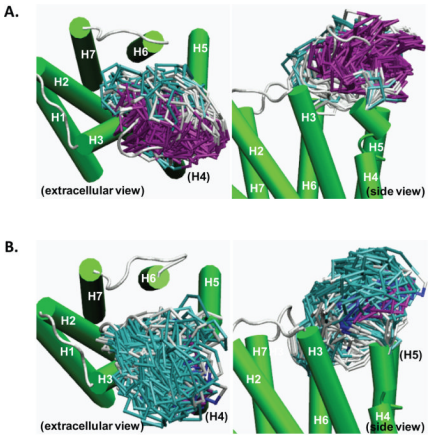

FIGURE 1.

Sampled conformations of E2 of the CB_1 receptor in a POPC bilayer by the SA simulation. **A**. Superposition of 166 conformations of $E2_{dithiol}$, with extracellular top view and side view. **B**. Superposition of 115 conformations of $E2_{disulfide}$, with extracellular top view and side view. Only C_α atoms of E2 are shown for clarity. The TM helical bundle is represented in green cartoon, while the extracellular loops are colored according to the secondary structure: α-helix, purple; 3_{10} helix, blue; turn, cyan; and coil, white.

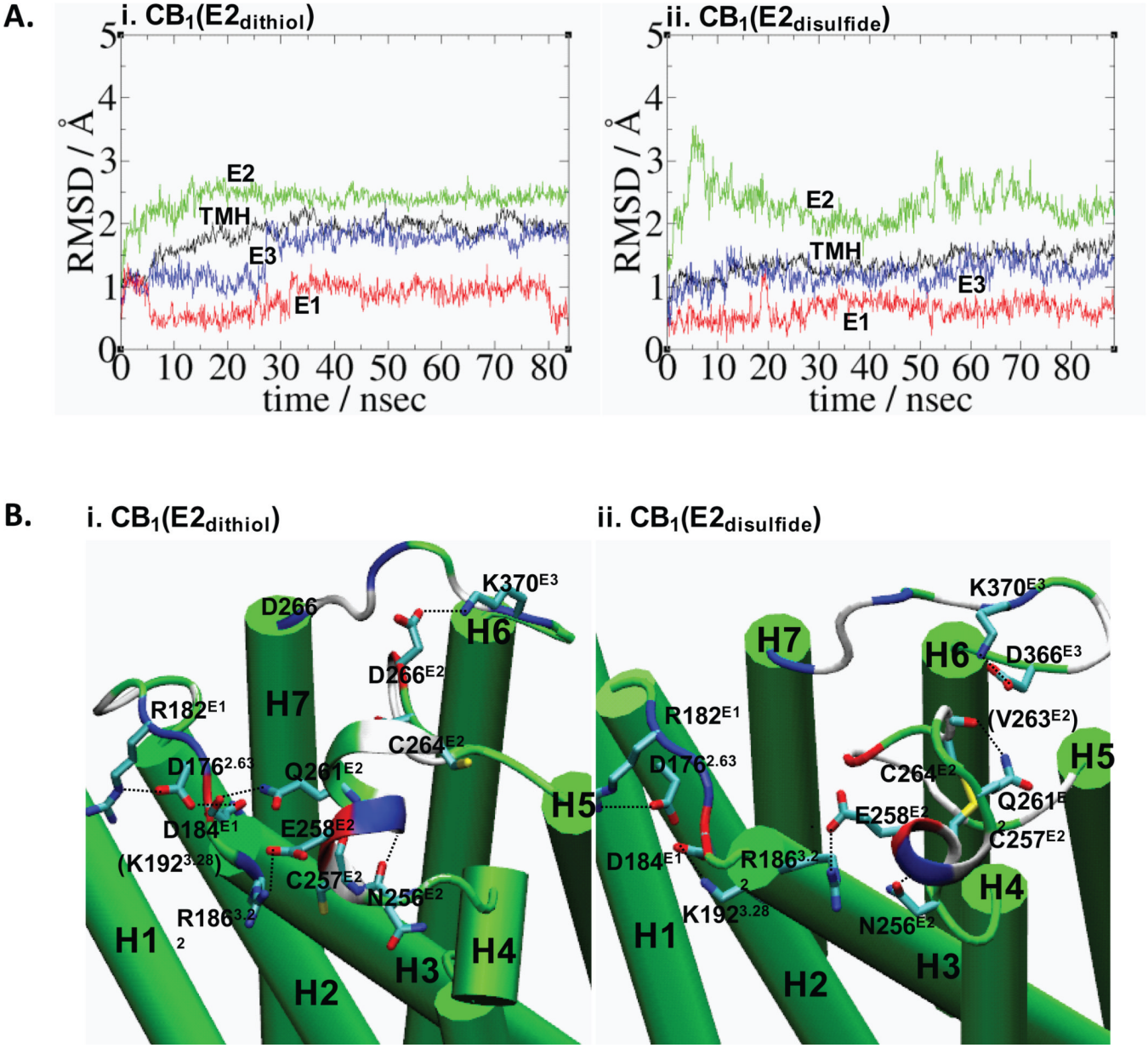

FIGURE 2.

MD simulations of $CB_1(E2_{dithiol})$ conformation **A1** for a total of 83 ns duration and $CB_1(E2_{disulfide})$ conformation **B3** for a total of 88 ns duration. **A**. The RMSDs for $CB_1(E2_{dithiol})$ (i) and for $CB_1(E2_{disulfide})$ (ii), calculated by RMS fitting to the initial coordinates with respect to the backbone heavy atoms of the receptor TM helical residues: TMH, black; E1, red; E2, green; and E3, blue. The TM helical and extracellular loop boundaries of $CB_1(E2_{dithiol})$ are defined as follows: H1, $P113^{1.29}$-$H143^{1.59}$; H2, $P151^{2.38}$-$D176^{2.63}$; H3, $R186^{3.22}$-$H219^{3.55}$; H4, $R230^{4.39}$-$L253^{4.62}$; H5, $I271^{5.35}$-$H302^{5.66}$; H6, $M337^{6.29}$-$F368^{6.60}$; H7, $K376^{7.32}$-$Y397^{7.53}$; E1, $F177^{E1}$-$D184^{E1}$; E2, $G254^{E2}$-$H270^{E2}$ and E3, $G369^{E3}$-$I375^{E3}$. Similarly, the TM helical boundaries of $CB_1(E2_{disulfide})$ are defined as follows: H1, $P113^{1.29}$-$H143^{1.59}$; H2, $P151^{2.38}$-$V179^{2.66}$; H3, $R186^{3.22}$-$H219^{3.55}$; H4, $R230^{4.39}$-$G254^{4.63}$; H5, $D272^{5.36}$-$R311^{5.75}$; H6, $M337^{6.29}$-$F368^{6.57}$; H7, $T377^{7.33}$-$Y397^{7.53}$; E1, $F180^{E1}$-$S185^{E1}$; E2, $W255^{E2}$-$I271^{E2}$ and E3, $D366^{E3}$-$K376^{E3}$ **B**. The extracellular loop

region in $CB_1(E2_{dithiol})$ (i) and $CB_1(E2_{disulfide})$ (ii) at the end of the MD simulation. The extracellular loop residues (colored according to the atom type) participating in salt bridges and E2 H-bonds (by dotted lines) are shown (see Table III). Hydrogen atoms as well as some side chains are omitted for clarity. The E2 α-helical segment is represented in ribbon, while all other residues are in cartoon. TMH are colored in green while the extracellular loops are colored according to the residue type: hydrophobic, white; hydrophilic, green; positively charged, blue; and negatively charged, red.

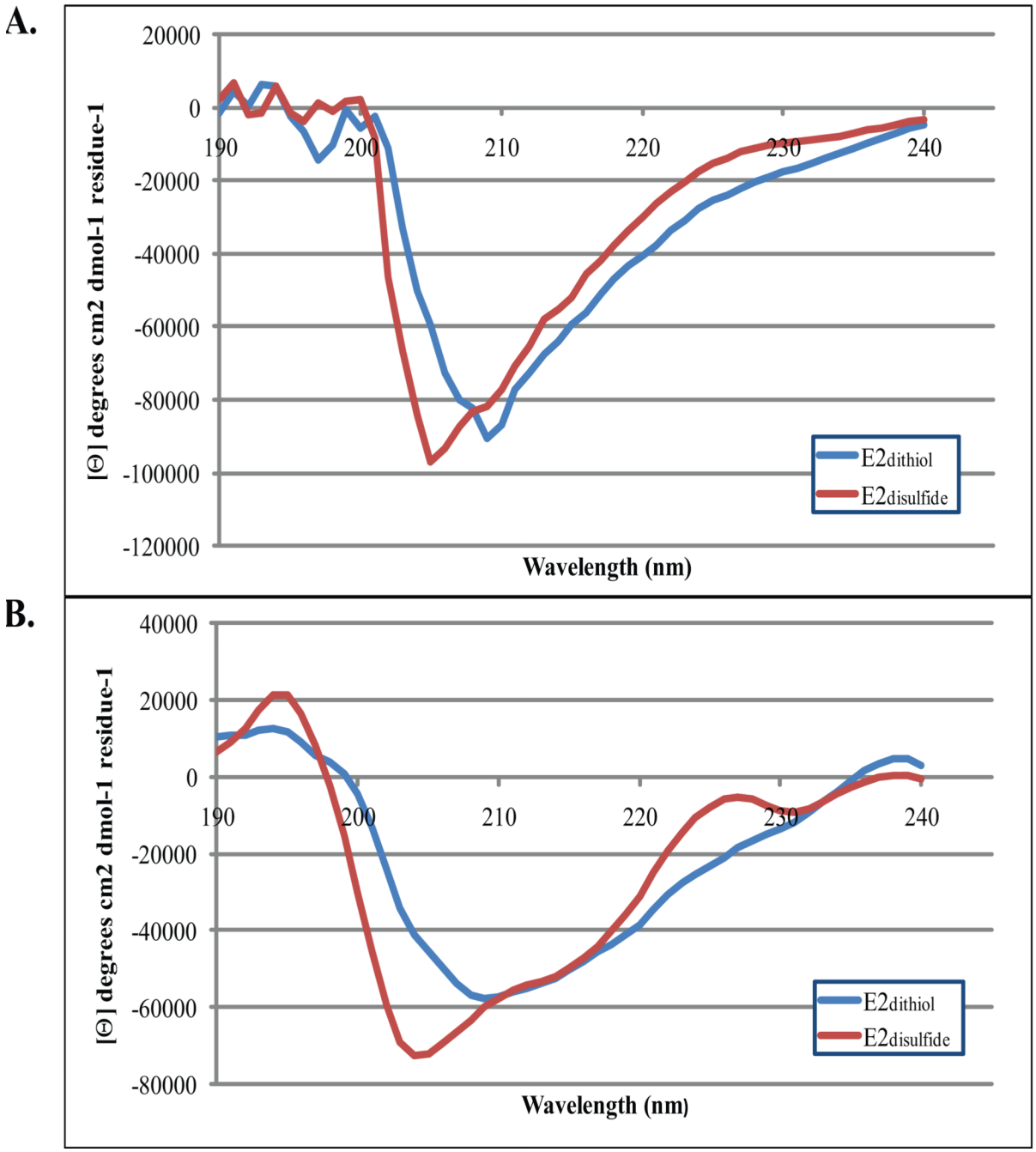

FIGURE 3.

Circular dichroism spectroscopy of peptide fragments of $E2_{dithiol}$ and $E2_{disulfide}$ **A**. Far UV CD spectra of the $E2_{dithiol}$ (in blue) and $E2_{disulfide}$ (in red). CD-bands with mean residue ellipticities ([Θ]-values) that are positive at 195 nm and negative at 209 nm are visible in both spectra indicative of α-helix formation by both $E2_{dithiol}$ and $E2_{disulfide}$. The 222 nm band typical of α-helicies is barely visible in these spectra. The strong negative band at 205 nm in the $E2_{disulfide}$ spectrum remains to be explained. **B**. Deconvolution of the CD-spectra further indicates that α-helical secondary structure elements contribute to the CD-spectrum of $E2_{dithiol}$. All three bands typical of α-helical secondary structure are visible, including the band at 222 nm. Deconvolution of the CD-spectrum for $E2_{disulfide}$ did not yield any

additional information about the secondary structure although α-helix formation is likely also in this peptide as indicated by the positive and negative [Θ]-values at 195 nm and 209 nm respectively. Output from CONTIN L show that α-helix contributes to 80 % of the $E2_{dithiol}$ secondary structure.

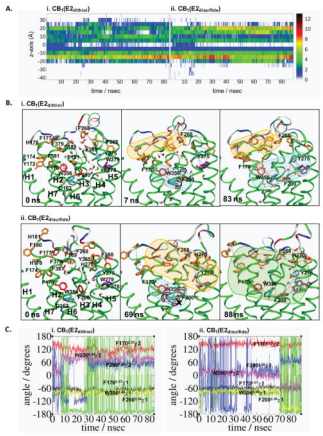

FIGURE 4.

Aromatic stacking interactions in $CB_1(E2_{dithiol})$ and $CB_1(E2_{disulfide})$. **A**. Concentration of aromatic stacking during the 83 ns MD simulation of $CB_1(E2_{dithiol})$ (i) and the 88 ns simulation of $CB_1(E2_{disulfide})$ (ii). Aromatic stacking was defined as any two aromatic residues (F, Y, W, or H) for which the centroid to centroid distance was < 8.0 Å. Z-axis position of each stack was determined by the z coordinate of one participating residue. The concentration of aromatic stacking is plotted in ranges of 5 Å with the concentration indicated by the following colors in decreasing order: black, red, orange, yellow, green, blue and white (no aromatic stacking). **B**. The aromatic stacking (by dotted lines) networks in $CB_1(E2_{dithiol})$ (i) and $CB_1(E2_{disulfide})$ (ii). The snapshot at 6 ns of the simulation of $CB_1(E2_{dithiol})$, when the $W356^{6.48}$ indole ring flipping occurs (i.e., the χ2 angle changes from ~ 0 degree to ~ +70 degrees), and the snapshot at 26 ns of the simulation of $CB_1(E2_{disulfide})$, when the $W356^{6.48}$ indole ring flipping occurs (i.e., the χ1 angle changes from ~ −70 degree to ~ −150 degrees and the χ2 angle changes from ~ 0 degree to ~ −70 degrees), are shown in addition to the snapshots at the beginning and at the end of the simulations. The toggle switch $W356^{6.48}$ is circled (in red dot). Only the side chains of these aromatic residues, without H atoms, are shown. The water molecules located within 12 Å of $W356^{6.48}$ are also shown. The aromatic stacking networks are indicated by the circles: the network around $F268^{E2}$ and $H270^{E2}$, orange; the network around $W356^{6.48}$, blue; and the network combining these two networks through $H270^{E2}/Y275^{5.39}$ aromatic stacking, in green. Color coding for the protein (in cartoon) is the same as in Fig. 2. **C**. The χ1 and χ2 angles of $F170^{2.57}$, $F200^{3.36}$ and $W356^{6.48}$ during the duration of 83 ns MD simulation for $CB_1(E2_{dithiol})$ (i) and during the duration of 88 ns MD simulation for $CB_1(E2_{disulfide})$ (ii). Color coding: the χ1 angle of $F170^{2.57}$, black; the χ2 angle of $F170^{2.57}$, red; the χ1 angle of $F200^{3.36}$, green; the χ2 angle of $F200^{3.36}$, blue; the χ1 angle of $W356^{6.48}$, yellow; and the χ2 angle of $W356^{6.48}$, magenta.

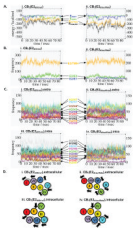

FIGURE 5.

Modifications of the helical topology caused by the inter-molecular interactions with distinct E2 structures of the CB_1 receptor. **A**. Non-bonding interaction energies (in kcal/mol), which is a summation of the electrostatic and the van der Waals components, between E2 and the other parts of the receptor ($E_{inter,E2}$) (in black), including E1 ($E_{E2/E1}$) (in blue), E3 ($E_{E2/E3}$) (in green) and TMH ($E_{E2/TMH}$) (in orange), are displayed for $CB_1(E2_{dithiol})$ (i) and for $CB_1(E2_{disulfide})$ (ii). **B**. The contact numbers between E2 and E1 (in blue), E3 (in green) or TMH (in orange) in $CB_1(E2_{dithiol})$ (i) and $CB_1(E2_{disulfide})$ (ii). A criterion of 3.5 Å was used between non-bonded atoms. **C**. The contact numbers between TMH in the extracellular half of $CB_1(E2_{dithiol})$ (i) and $CB_1(E2_{disulfide})$ (ii) and in the intracellular half of $CB_1(E2_{dithiol})$ (iii) and $CB_1(E2_{disulfide})$ (iv). A criterion of 3.5 Å was used between non-bonded atoms. Color coding: H1/H2, black; H1/H7, red; H2/H3, green; H2/H4, blue; H2/H7, yellow; H3/H4, brown; H3/H5, grey; H3/H6, violet; H4/H5, magenta; H5/H6, orange; and H6/H7, turquoise. **D**. The extracellular TM helical bundle structures of $CB_1(E2_{dithiol})$ (i) and $CB_1(E2_{disulfide})$ (ii) and the intracellular helical bundle structures of $CB_1(E2_{dithiol})$ (iii) and $CB_1(E2_{disulfide})$ (iv) predicted by their contact numbers are shown in comparison with the CB_1 receptor model[32] whose TM helical bundle structure was same both in $CB_1(E2_{dithiol})$ and $CB_1(E2_{disulfide})$ at the beginning of the respective simulations. The TM helical boundaries of the CB_1 receptor are defined same as in Fig. 3. Color coding for the TMH (in ribbon): H1, red; H2, orange; H3, yellow; H4, green; H5, cyan; H6, blue; and H7, purple.

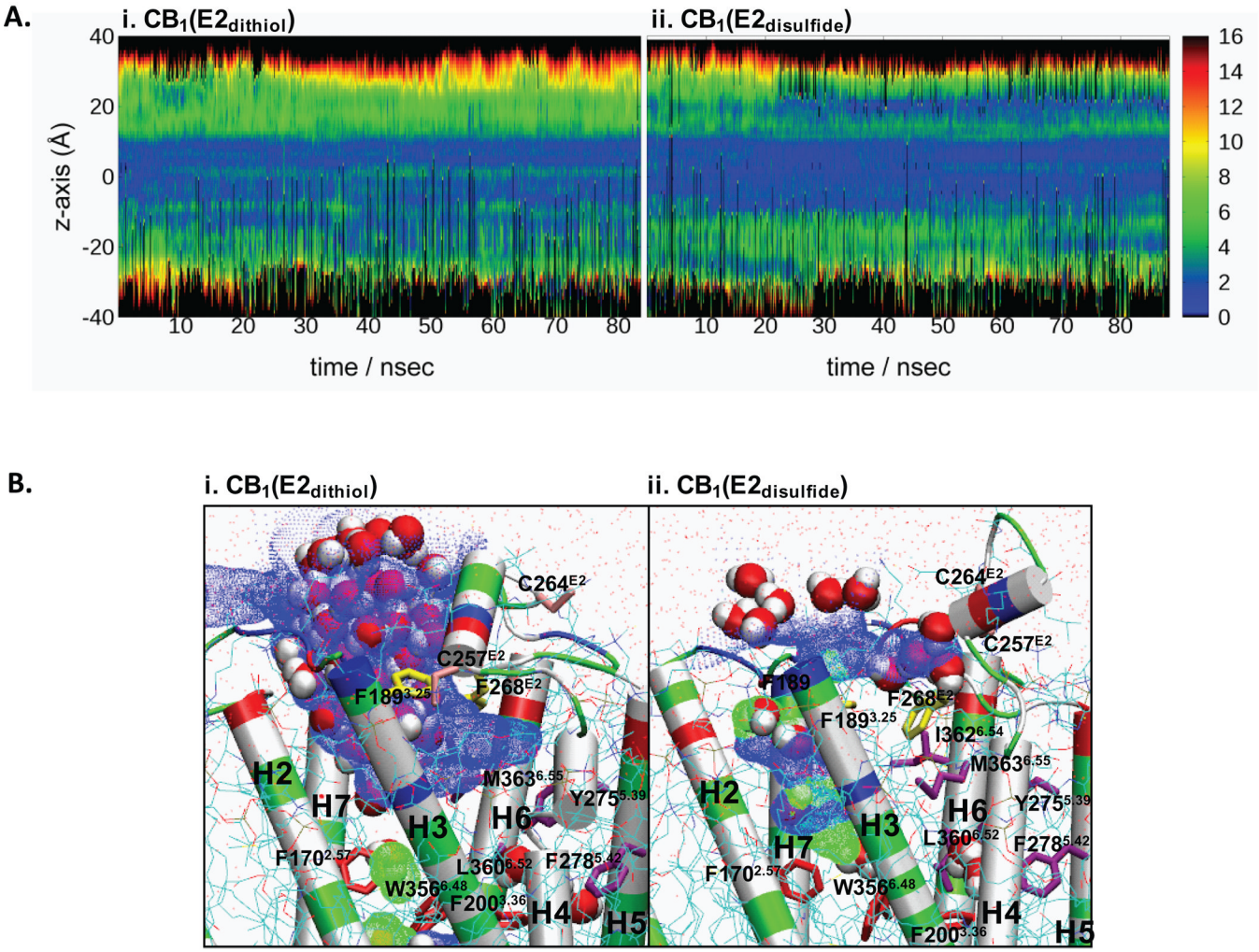

FIGURE 6.

Core crevice analysis of $CB_1(E2_{dithiol})$ and $CB_1(E2_{disulfide})$. **A**. Pore diameter along the Z axis during the 83 ns MD simulation of $CB_1(E2_{dithiol})$ (i) and the 88 ns simulation of $CB_1(E2_{disulfide})$ (ii). Colors indicate the diameter of the pore in angstroms (red: 14 Å; orange: 12 Å; yellow; 9 Å etc.). Pore diameter was determined using HOLE with sampling done every 0.5 Å along the z-axis; a midpoint between H3 and H7 was used to help define the pore (c-point). **B**. The solvent accessible pore (in blue dots for low radius surface and in green dots for mid radius surface) created by using HOLE at the extracellular core region in $E2_{dithiol}$ (i) at the end of 83 ns of MD simulation and in $E2_{disulfide}$ (ii) at the end of 88 ns of MD simulation. Color coding for residues (in stick): the residues forming the aromatic cluster at the top of the extracellular pore region, yellow; $F189^{3.25}$ and $F268^{E2}$, located at the entrance of the pocket and known as crucial for ligand recognition,[56,61]; the residues forming the water-accessible binding surface in the CB_2 receptor,[30] purple; and $F170^{2.57}$, $F200^{3.36}$ and $W356^{6.48}$, red. Colored according to the atom type, water molecules inside and outside the receptor crevice are represented in space filling and line, respectively, while the lipid molecules are represented in lines. Color coding for the protein (in cartoon): hydrophobic, white; hydrophilic, green; positively charged, blue; and negatively charged, red.

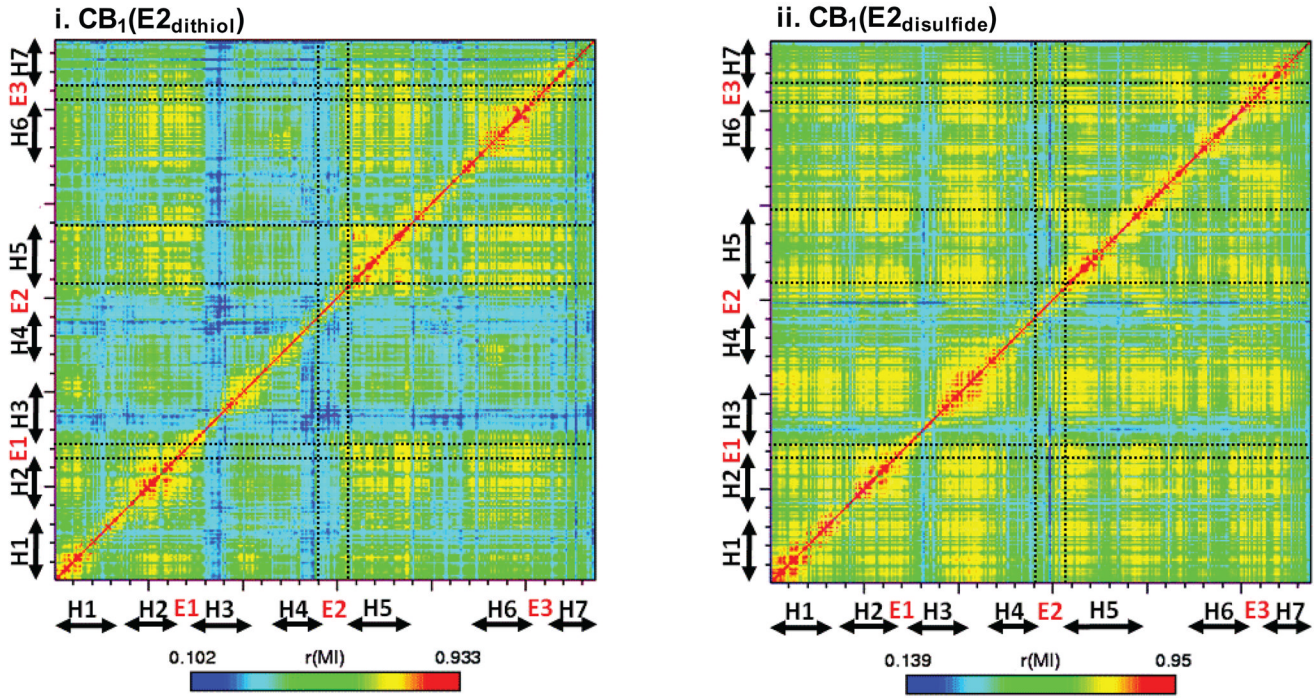

FIGURE 7.

Cross correlation of $CB_1(E2_{dithiol})$ and $CB_1(E2_{disulfide})$. X- and y-axes are the receptor H1 through H7; red indicates highly correlated movement (1.0) and blue indicates less correlated (0.0). The E2/H5 correlation is indicated by a dotted circle. Cross correlation was performed with g_correlation [52] to create cross-correlation matrices from ~ 12,000 coordinates recorded every 2 ps from the last 24 ns MD simulations of $CB_1(E2_{dithiol})$ and $CB_1(E2_{disulfide})$, respectively.

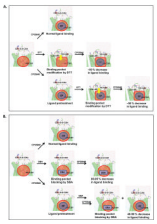

FIGURE 8.

The role of E2 disulfide bond of the CB_1 receptor in modification of ligand binding. **A**. The modification of the binding of CP55940 (as indicated by the blue circle) to the CB_1 receptor by dithiothreitol (DTT). The observed 50 % decrease in CP55940 binding affinity,[31] regardless of the pretreatment of CP55940, by DTT is due to indirect modification of the binding pocket, schematically shown from the red circle to the red square shape in the TM core induced (as indicated by the yellow arrow) by E2 conformational change as its disulfide bond is reduced to free thiols. **B**. The modification of the binding of CP55940 to the CB_1 receptor by sulfhydryl blocking agents (SBAs) (as indicated by the blue rectangle). Pretreatment of CP55940 significantly attenuates the effects of SBAs, which reduce CP55940 binding affinity;[31] this can be interpreted as the protection of the binding pocket by CP55940 without or with little modification of the binding pocket by SBAs. Explanation is based upon the suggestions of the present studies that $E2_{disulfide}$ is the biologically relevant form and that a conformational change caused by the reduction of E2 disulfide bond can modify the ligand binding pocket.

Table I

Secondary structure prediction of E2 of β_1AR, β_2AR, A_{A2}R, and the CB_1 receptor by various prediction programs

Prediction method	Sequence and secondary structure[f]			
	β_1AR		β_2AR	
	Start	End	Start	
	181	204	173	
	WWRDEDPQALKCYQDPGCCDFVTN		**WYRATHQEAINCYAEETCCDFFTN**	
PSIPRED[a]	EEECCCHHHHHHCCCCCCCCCCCC		EEECCCHHHHHHHCCCCC	
JPRED3[bc]	------HHHHH----------		-E----HHHHH----------	
APSSP2[d]	CECCCCHHHHHHHCCCCCCCCCC		ECCCCCHHHHHCCCCCCECECCC	
X-ray[e]	TTE---HHHHHHHH-TT-----E-		TT----HHHHHHH--TT-	
	A_{A2}R		CB_1	
	Start	End	Start	
	143	173	255	
	WNNCGQPKEGKNHSQGCGEGQVACLFEDVVP		**WNCEKLQSVCSDIFPHI**	
PSIPRED[a]	CCCCCCCCCCCCCCCCCCCCEEEEEEEEEE		CCHHHHHHHHHHHCC	
JPRED3[bc]	--------------------EEEEEE-----		---HHHHHHH-------	
APSSP2[d]	CCCCCCCCCCCCCCCCCCCCEEEEEECCCC		CCHHHHHHHHHHHH	
X-ray[e]	------------------TT-EE--HHHHH-			

[a] Ref. 23.

[b] Ref. 24.

[c] Based on a consensus from several methods, including DSC, PHD, NNSSP, PREDATOR, ZPRED, and MULPRED.

[d] Ref. 25.

[e] The E2 secondary structures, assigned by DSSP,[78] are taken from the X-ray β_1AR,[16] β_2AR[15] and A_{A2}R.[17]

[f] Estimated secondary structure codes: H, α-helix (shaded); E, extended (β-sheet); C, coil; and T, turn.

Table II

The number of the structure at each step of the conformational search procedure for the determination of $CB_1(E2_{dithiol})$ and $CB_1(E2_{dithiol})$

	i. step 1	**ii. step 2**			**iii. step 3**	**iv. step 4**
	SA no. of conf.	**cluster analysis no. of cluster**			**MD no. of conf. (time)**	**further MD no. of conf. (time)**
	sampled	obtained	retained		explored	explored
$E2_{dithiol}$	166	16	8	$CB_1(E2_{dithiol})$	16[a] (5 ns)	4 (**A1, A2, B1** & **A3**) (8 – 78 ns)
$E2_{disulfide}$	115	28	11	$CB_1(E2_{disulfide})$	12[b] (10 ns)	4 (**B2, B3, B4** & **B5**) (0 – 78 ns)

[a] A total of 16 different $E2_{dithiol}$ conformations in 8 clusters (5, 4, 2, 1, 1, 1, 1, and 1) were used to derive 16 different $CB_1(E2_{dithiol})$ models.

[b] A total of 12 different $E2_{disulfide}$ conformations in 11 clusters (2, 1, 1, 1, 1, 1, 1, 1, 1, and 1) were used to derive 12 different $CB_1(E2_{disulfide})$ models.

Table III

Molecular interactions in $CB_1(E2_{dithiol})$ and $CB_1(E2_{dithiol})$ at the receptor extracellular region

	$CB_1(E2_{dithiol})$	**$CB_1(E2_{disulfide})$**
salt bridge[a]	$D176^{2.63}/R182^{E1}$	$D176^{2.63}/R182^{E1}$
	$D176^{2.63}/K192^{3.28}$	$K183^{E1}/D266^{E2}$
	$D184^{E1}/K192^{3.28}$	$D184^{E1}/K192^{3.28}$
	$R186^{3.22}/E258^{E2}$	$R186^{3.22}/E258^{E2}$
	$D266^{E2}/K370^{E3}$	$D366^{6.58}/K370^{E3}$
H-bonding[b]	$D184^{E1}$ O(back)/$Q261^{E2}$ N(side)	$N256^{E2}$ O(side)/$K259^{E2}$ N(back)
	$N256^{E2}$ O(back)/$L260^{E2}$ N(back)	$N256^{E2}$ O(back)/$L260^{E2}$ N(back)
	$C257^{E2}$ O(back)/$Q261^{E2}$ N(back)	$C257^{E2}$ O(back)/$Q261^{E2}$ N(back)
	$V263^{E2}$ O(back)/$S265^{E2}$ N(back)	$E258^{E2}$ O(side)/$R186^{3.22}$ N(side)
aromatic stacking[c]	$F174^{2.61}$/ $F177^{2.64}$	$F177^{2.64}/F189^{3.25}$
	$F174^{2.61}$/ $H178^{2.65}$	$F177^{2.64}/F379^{7.35}$
	$F174^{2.61}$/ $F381^{7.37}$	$H178^{2.65}/H181^{2.68}$
	$F177^{2.64}$/ $F268^{E2}$	$H178^{2.65}/F381^{7.37}$
	$F177^{2.64}/F379^{7.35}$	$F180^{2.67}/H181^{2.68}$
	$H178^{2.65}$/ $F381^{7.37}$	$F189^{3.25}/F268^{E2}$
	$F189^{3.25}$/ $F268^{E2}$	$F189^{3.25}/F379^{7.35}$
	$F268^{E2}/Y275^{5.39}$	$F268^{E2}/H270^{E2}$
	$F268^{E2}/F379^{7.35}$	$F268^{E2}/Y275^{5.39}$
	$Y365^{6.57}/F368^{6.60}$	$F268^{E2}/F379^{7.35}$
		$H270^{E2}/Y275^{5.39}$
		$Y365^{6.57}/F368^{6.60}$

[a] Estimated by measuring the distance between the side chain O atom of a negatively charged residue and the side chain N atom of a positively charged residue with the cut-off distance of 3.20 Å.

[b] side, side chain; back, backbone

[c] Estimated by measuring the centroid to centroid distance between any two aromatic residues (Phe, Tyr, Trp, or His) with the cut-off distance of 8.0 Å.